CFSRC COLLOQUIUM

Proceedings of the Cold-Formed Steel Research Consortium Colloquium
20-22 October 2020 (cfsrc.org)

Direct strength method for web crippling of lipped channel sections with flanges restrained under ETF and ITF loadings

Zhi Qiao[1], Chao Li[3],Weihui Zhong[1,2]

Abstract

Web crippling is a prominent failure mode of cold-formed thin-walled steel members. In this study, a direct strength method (DSM) is investigated for the web crippling calculation of lipped channel sections with flanges restrained under the end-two-flange and interior-two-flange loading conditions. First, numerical models are utilised to obtain the elastic buckling critical load and plastic failure mechanism. Then, through correction, the elastic buckling critical load formula is established based on the elastic plate stability theory analysis. The plastic load formula is then deduced by assuming a yield-line mode under the limit state and using the virtual work principle. Based on parameter studies, the undetermined coefficients of the DSM are calculated. Finally, existing test results are compared with those of the proposed formula and AISI S100-16 calculation values, and the proposed formula achieves better results, highlighting its potential to provide reference values for engineering applications.

1. Introduction

Cold-formed thin-walled crimped C-section components are usually applied as floor beams and purlins for light steel houses. However, installing the transverse stiffeners is difficult and uneconomical due to the crimped cross-sections. Consequently, cold-formed steel beams usually lack stiffeners at bearings or concentrated load sites, thereby necessitating determination of the local compressive bearing capacity of the web during designing. The mainstream design codes in the world such as the AISI S100[1] of North America, AS/NZS 4600[2] of Australia/New Zealand and EC3:Parts 1–3[3] of the European Union provide a unified method for solving the web buckling problem. Some studies[4-7], however, report major errors between the predicted values from current standard formulae and measured values. For example, the experimental study by Young and Hancock[5] on a non-crimped C-section under end-two-flange (ETF) and interior-two-flange (ITF) conditions produced corresponding bearing capacities of just 63% and 57% of the calculated values from the AISI S100 code, suggesting usage of the standard formula requires caution. Therefore, revision is needed for the standard formulas.

In recent years, researchers have attempted to introduce a Direct Strength Method (DSM) for solving local web compression problems, with the method yielding good in predicting test results. Durate and Silvestre[8] proposed a design method based on the regularised slenderness ratio λ (ratio of the first-order plastic load to the elastic critical buckling load) for a non-crimped C-section in 2013. Subsequently, Keerthan et al.[9] investigated the web buckling capacity of a C-section with a hollow flange under ETF and ITF conditions, and they further developed the DSM based on the critical buckling load and first-order plastic load. Natário et al.[10-11] improved the critical buckling load required by the DSM, particularly for the ETF and ITF loading conditions. Further, the GBTWEB software was developed based on the general beam theory[12-13] for buckling analysis, and Sundararajah et al.[14-15] provided experimental data supporting the DSM improvement.

Nevertheless, the DSM still exhibits limitations. In practical engineering, the flange is often connected to the bearing plate at the bearing and the load action point, thereby restricting its rotation. According to the analysis by Gerges and Schuster[16], the buckling capacity improvement by this method cannot be ignored. However, the study involved few experiments, and the finite element analysis for this connection mode and the correspondence with the DSM theory and its application was limited. Hence, to improve the basic theoretical and engineering applications of the DSM, this study involves examining the local pressure-

[1]School of Civil Engineering, Xi'an University of Architecture & Technology, Xi'an 710055, China
[2]Key Lab of Structure Engineering and Earthquake Resistance (XAUAT), Xi'an 710055, China
[3]CITIC General Institute of Architectural Design and Research Institute Co., Ltd, Wuhan 430014, China

bearing performance of a crimped C-section under the ETF and ITF conditions and providing corresponding calculation methods.

2. Numerical Model and Parameter Analysis

In this study, the nonlinear finite element analysis software ABAQUS was utilised for analysing the local pressure-bearing performance of a crimped C-section under ETF and ITF conditions, with the results of Uzzama[17,18] considered the basis for validating the finite element model. Meanwhile, according to the correct numerical model, the parameter range of the physical experiment was expanded through parametric analysis, and the results support the formulas introduced.

2.1 Establishment and verification of numerical models

Figures 1 and 2 are finite element models of specimens under the ETF and ITF conditions, respectively. The boundary conditions are identical, despite the specimen length difference between the two stress conditions. The shell element S4R was selected for simulating a C-shaped sectional test piece. This is because the thickness of its bearing plate largely surpasses that of the specimen and its deformation during loading is low. In addition, the rigid body element R3D4 was selected for simulation. The material properties of the specimen were adopted from the original study [17,18]. The binding constraint (*Tie) was exploited for simulating the bolt connection between the bearing plate and the flange in the 10 mm × 10 mm area in the middle of the rigid body's bearing plate at the upper and lower flanges of the specimen. In defining the contact property, the isotropic Coulomb contact in the tangential direction was utilised, with the friction coefficient set to 0.3. A soft contact was involved in the normal direction and the pressure contact curve was linear, with a selected linear stiffness of 4000 kN/m. The upper and lower rigid body bearing plates were then coupled to the reference points RP-1 and RP-2, respectively, with boundary constraints imposed as shown in Figures 1 and 2.

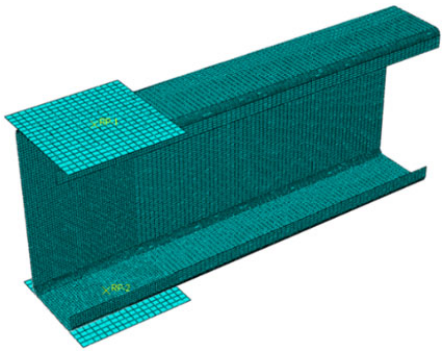

Figure 1: Finite element model for a specimen under the ETF working condition

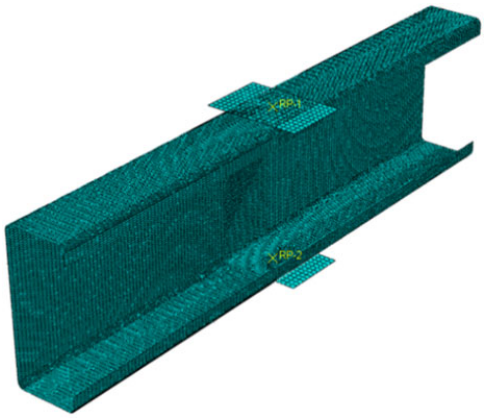

Figure 2: Finite element model of a specimen for the ITF working condition

Comparing the local compressive bearing capacity of the specimens obtained from the test and finite element analysis under the ETF and ITF conditions, the numerical analysis results under both conditions are slightly higher than the test values, with average errors of 6.6% and 1.7%, respectively. However, the calculation errors of the numerical models are considered to be within a reasonable range.

2.2 Parametric analysis

In this study, the geometric parameters of C-section components such as the inner bending radius r_i, the web height h_w and the supporting length N were analysed by the dimensionless variable parameters. Meanwhile, considering the nonlinearity of the materials, three steel grades including the Q235, Q345, and Q390 (representing yield strengths (f_{ys}) of 235, 345, and 390 MPa, respectively) were selected, with the values for each parameter listed in Table 1.

Table 1: Parameter values for various inner bending radius, web height, and yield strength

$h \times b_f \times b_L \times t$	r_i(mm)	N(mm)	f_y(MPa)
100×50×15×2.5	4.5	50	235
140×50×20×2.0			
180×70×20×2.0	5.5	100	345
200×70×20×3.0	7.0	150	390
220×75×25×2.5			
300×80×25×3.0			

Note: $h \times b_f \times b_L \times t$ represents the total web height × flange width × hemming height × plate thickness.

3. Recommended Formula Based on the Direct Strength Method

The DSM was proposed by Schafer and Pekoz[19] in 1998. This method mainly considers the relationship between the

limit state and the single failure mode of components such as the yield and elastic buckling to establish a calculation formula, as shown in Equation 1.

$$R_{\mathrm{b}}=R_{\mathrm{b}}\left(R_{\mathrm{b,cr}}, R_{\mathrm{b,y}}\right) \tag{1}$$

From a theoretical perspective, when cold-formed thin-walled steel components are under local transverse loads, the stiffness degradation caused by the elastic instability of the web and the cross-sectional strength weakening associated with the plastic distribution produce local buckling of the web. This is consistent with the DSM application conditions. To obtain a DSM-based formula, the critical buckling load $R_{\mathrm{b,cr}}$ and plastic load $R_{\mathrm{b,y}}$ calculation methods must be initially developed.

3.1 Critical buckling load $R_{b,cr}$ calculation method

Figure 3 is a schematic diagram of simply supported rectangular plates bearing local distributed loads on opposite sides. According to the classical elastic plate stability theory, the critical elastic buckling load $R_{\mathrm{b,cr}}$ of such a plate under edge loading can be expressed by Equation 2, with the buckling coefficient k_{f} associated with the load form, boundary conditions, and plate size.

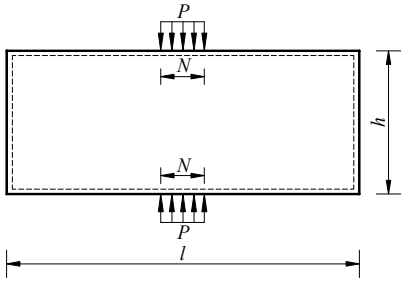

Figure 3: Simply supported plate with opposite edges bearing local distributed loads

$$R_{\mathrm{b,cr}}=k_{\mathrm{f}}\cdot\frac{\pi^2 E}{12(1-\upsilon^2)}\frac{t^3}{h} \tag{2}$$

Here, E and υ are the elastic modulus and Poisson's ratio, respectively of steel.

In this study, the object is a crimped C-section, and the load is often transferred by a fillet at the joint between the flat section of the web and flange. This is not equivalent to the so-called simply-supported boundary condition. Therefore, the buckling coefficient obtained from the plate stability theory is not directly applicable for calculating the elastic critical buckling load required. Hence, based on Equation 2, the actual boundary constraint of the web and the stress conditions difference require consideration in expressing the buckling coefficient kf. Duarte and Silvestre[8] revised the buckling coefficient kf of the C-section web under locally distributed loads on both sides proposed in earlier studie [20], as shown in Equation 3.

$$k_{\mathrm{f}}=\left(1+c_1\cdot\frac{N}{h}\right)\left[c_2+c_3\cdot\left(\frac{h}{l}\right)^2+c_4\cdot\sqrt[4]{\frac{b_{\mathrm{f}}}{h}}\right] \tag{3}$$

Here, C_1, C_2, C_3, and C_4 are the undetermined coefficients needed for determining the buckling coefficients under various working conditions.

The eigenvalue buckling analysis of the crimped C-section components under ETF and ITF was performed using the ABAQUS software. Following the application of a unit load, the buckling factor corresponding to the lowest order buckling mode is considered the critical buckling load $R_{\mathrm{b,cr}}$. Using the MATLAB software for regression analysis, the undetermined coefficients in Equation 3 were obtained, as shown by the data presented in Table 2. The R^2 value for the evaluation index of the regression analysis exceeds 0.99.

Table 2: Summarised data for the undetermined coefficients in Equation 3 determined by regression analysis

Working condition	C_1	C_2	C_3	C_4
ETF	2.188	1.94	-1.466	-0.528
ITF	0.575	3.653	-2.696	-0.064

3.2 Plastic load $R_{b,y}$ calculation method

To understand the plastic mechanism of the local compression failure of the components, Mises equivalent stress nephograms corresponding to peak points of the load–displacement curves under the two working conditions were extracted. To obtain a simplified plastic mechanism model, the following assumptions are introduced in this study:

(1) the plastic hinges are distributed along a straight line in the longitudinal direction of the intersection between the web and the flange and the fillet; and

(2) the bending moment distribution of the plastic hinge is uniform along the yield-line.

Figures 4 and 5, respectively, display the Mises equivalent stress nephogram of specimens under the ETF and ITF conditions in the limit state, with these indicating that plastic regions exist in the web and flange positions when the specimens attain the limit state. According to the out-of-plane convex deformation mode of the cross-section, the double-arrowed solid line in the illustration can be considered its yield-line.

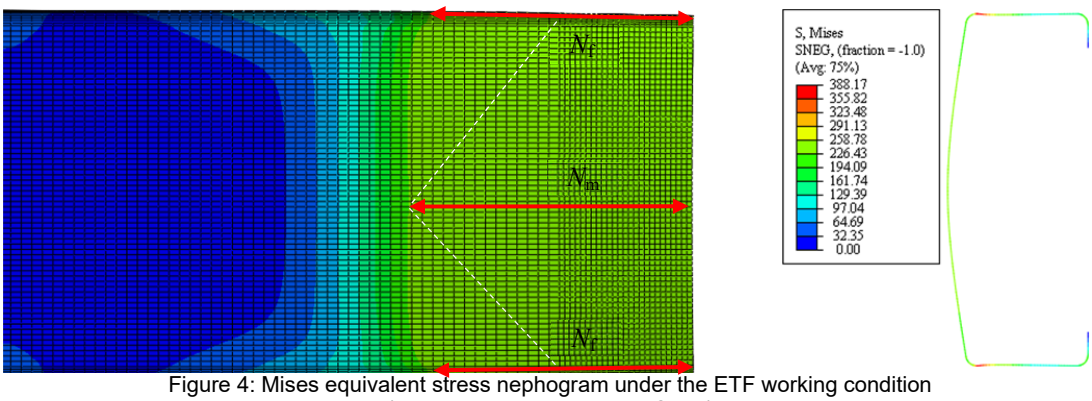

Figure 4: Mises equivalent stress nephogram under the ETF working condition (200×70×20×3.0×4.5N100-Q235)

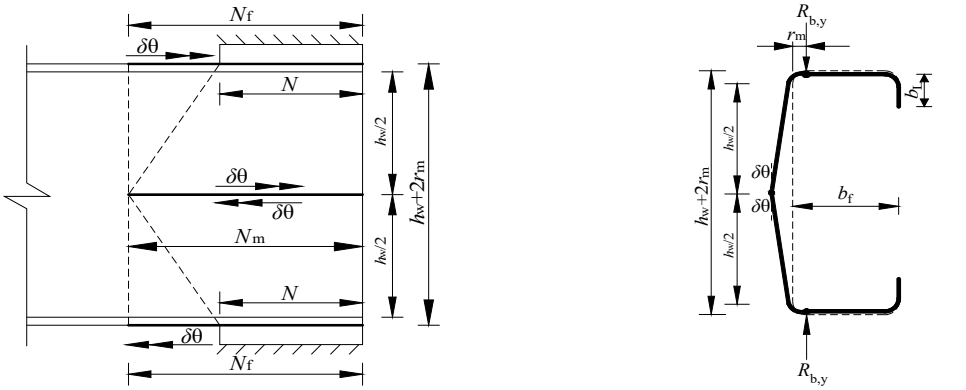

Figure 5: Mises equivalent stress nephogram under the ETF working condition (200×70×20×3.0×4.5N100-Q235)

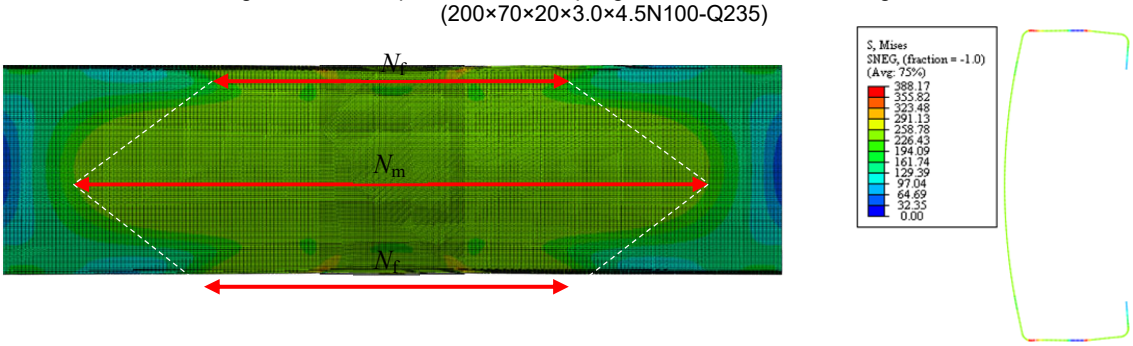

Figure 6: Typical Mises equivalent stress nephogram under the ITF working condition (C220×75×25×2.5×4.5N150-Q235)

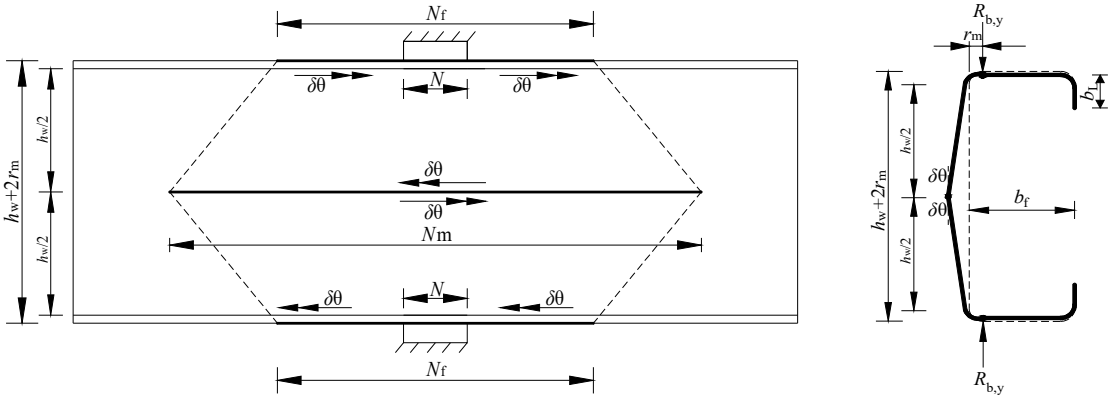

Figure 7: Illustration of an assumed yield-line mode under the ITF condition

The yield-line modes under the ETF and ITF conditions assumed in this study are displayed in Figures 5 and 7, with all dimensions expressed relative to the midline. According to the out-of-plane deformation mode and stress nephogram of the web, the yield-line develops in the middle of the web. Since the flange is connected to the support plate, when the web is deformed out-of-plane, the rotation of the flange is limited. This creates a plastic strand in the longitudinal direction of the intersection between the upper and lower flanges and the fillet. The length of the middle horizontal solid line is called the yield mechanism length N_m of the web, while the length of the upper or lower horizontal solid line is referred as the yield mechanism length N_f of the flange. The yield mechanism length can be measured through the Mises equivalent stress nephogram in the limit state. Statistical analysis demonstrates that the influence of the yield strength on the yield mechanism length is minor, and so, the latter can be approximated by the average of three values. The lengths N_f and N_m of the yield mechanism are related to the supporting length N, the radius of the middle line r_m and the height of the straight section of the web h_w. In this study, linear superposition relationships are assumed, as shown in Equations 4 and 5, where *a* to *f* are undetermined coefficients, and the calculation formula can be obtained by regression analysis.

According to Murray and Khoo[21], the plastic bending moment M_p of a cold-formed thin-walled plate is given by Equation 6, and the corresponding plastic hinge coupled to the axial force bending moment M_p is obtained from Equation 7. The formulas for calculating the plastic load under the ETF and ITF conditions given below are based on the virtual work principle.

$$N_m = a \cdot N + b \cdot h_w + c \cdot r_m \tag{4}$$

$$N_f = d \cdot N + e \cdot h_w + f \cdot r_m \tag{5}$$

$$M_P = \frac{f_y t^2}{4} \tag{6}$$

$$M_P^{'} = \left[1 - \left(\frac{R_{b,y}}{t N_m f_y} \right)^2 \right] M_p \tag{7}$$

The virtual work of the external force is given by:

$$\delta W_{external} = 2 R_{b,y} \cdot r_m \cdot \delta_\theta \tag{8}$$

while that of the internal force is expressed as follows:

$$\delta W_{internal} = 2 M_P^{'} \cdot N_m \cdot \delta_\theta + 2 M_P \cdot N_f \cdot \delta_\theta \tag{9}$$

According to the virtual work principle, the $\delta W_{external} = \delta W_{internal}$, and so, the following can be derived:

$$R_{b,y} \cdot r_m \delta_\theta = M_P^{'} \cdot N_m \cdot \delta_\theta + M_P \cdot N_f \cdot \delta_\theta \tag{10}$$

After sorting, the following can be derived:

$$R_{b,y}^2 + 4 r_m f_y N_m R_{b,y} - f_y^2 N_m^2 t^2 \left(1 + \frac{N_f}{N_m}\right) = 0 \tag{11}$$

Then, the calculation formula for the plastic load can be obtained finally as:

$$R_{b,y} = f_y N_m \left(\sqrt{4 r_m^2 + \left(1 + \frac{N_f}{N_m}\right) t^2} - 2 r_m \right) \tag{12}$$

Based on the statistical data from the parameter analysis, regression analyses were conducted for the yield mechanism lengths N_f and N_m data. Under the ETF condition, the statistical analysis data reveals that the length of the flange and web yield mechanism are almost equal, and $N_f = N_m$ is acceptable. The calculation is achieved through Equation 13, and yields an R^2 of 0.90.

$$N_m = N_f = 0.24 N + 0.55 h_w + 7.54 r_m \tag{13}$$

The yield mechanism lengths N_f and N_m under the ITF condition are obtained from Equations 15 and 16, respectively, with an identical R^2 value of 0.85.

$$N_m = 0.60 N + 1.54 h_w + 26.65 r_m \tag{14}$$

$$N_f = 0.94 N + 0.54 h_w + 12.84 r_m \tag{15}$$

3.3 Local compressive bearing capacity formula

Based on the DSM expressed in Equation 16, and the elastic critical buckling load $R_{b,cr}$ and plastic loads $R_{b,y}$ calculations, the undetermined coefficients *a*, *b* and *c* are obtainable from regression analysis of the parametric analysis data. The calculated data are presented in Table 3, with the recommended formulas shown as Equations 17 and 18.

$$\frac{R_b}{R_{b,y}} = a \left[1 - b \left(\frac{R_{b,cr}}{R_{b,y}} \right)^c \right] \left(\frac{R_{b,cr}}{R_{b,y}} \right)^c \tag{16}$$

$$\begin{cases} \dfrac{R_b}{R_{b,y}} = 1 \\ \dfrac{R_b}{R_{b,y}} = a\left[1 - b\left(\dfrac{1}{\lambda}\right)^{2c}\right]\left(\dfrac{1}{\lambda}\right)^{2c} \end{cases} \quad (17)$$

Table 3: Calculated data for the undetermined coefficients for the ETF and ITF conditions

Working condition	*a*	*b*	*c*	λ_0
ETF	0.50	0.119	0.482	0.362
ITF	0.56	0.090	0.308	0.271

Figures 8 and 9 display comparisons between the results from numerical analysis and the formula in Equation 17 proposed by the DSM under the ETF and ITF conditions. Evidently, in the correlation curve between the $R_b/R_{b,y}$ and the regularised slenderness ratio, except for a small amount of data in the upper part for which $R_b/R_{b,y}$=1 under the ETF condition, all other data exhibit $R_b/R_{b,y}$<1. This indicates that the plastic load $R_{b,y}$ proposed in this study is reasonable for the dimensionless ultimate bearing capacity, and clearly, the $R_b/R_{b,y}$ decreases with increasing regularised slenderness ratio. The regression curve converges with the data points, with R^2 values of 0.96 and 0.90 for the ETF and ITF, respectively. This further demonstrates the reliability of the formulas proposed in this study.

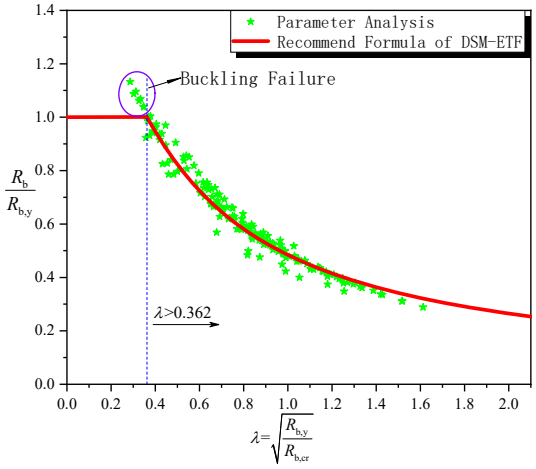

Figure 8: Comparison of the results from numerical analysis under the ETF condition and the DSM-based formula

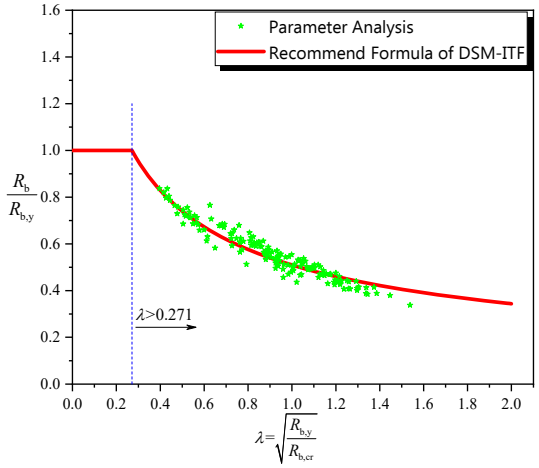

Figure 9: Comparison of the results from numerical analysis under the ITF condition and the DSM-based formula

4. Calculation Verification and Comparison

To verify the correctness of the proposed formula in Equation 17, test data from previous studies [17,18,22] were utilised. The relative errors between the results from the proposed formula, the North American standard formula in Equation 19 and the actual test results under the ETF and ITF conditions are presented in Table 4 and Table 5, respectively.

The unified expression in Equation 19 was adopted in the AISI S100-16 to calculate the local compressive bearing capacity R_b.

$$R_b = Ct^2 f_y \left(1 - C_R\sqrt{\frac{r_i}{t}}\right)\left(1 + C_N\sqrt{\frac{N}{t}}\right)\left(1 - C_h\sqrt{\frac{h_w}{t}}\right) \quad (19)$$

Here, C, C_R, C_N and C_h are coefficients associated with the section form, stress working condition and whether the flange is connected to the bearing plate. The specific value for a crimped C-section when the flange is restrained is available in [1].

Under the ETF and ITF stress conditions, all the results from the North American code are unreliable, with average errors reaching 25.94% and 42.20%, respectively. In contrast, the average errors from the formulas proposed in this study are within 10% and suitable for most cases. This demonstrates that the formulas are reasonable and reliable.

Table 4: Comparison of results from the recommended formula for the ETF condition and the North American standard formula

Model number	$R_{b,exp}$ (kN)	Recommended formula R_b (kN)	1-$R_b/R_{b,exp}$	$R_{b,AISI}$	1-$R_{b,AISI}/R_{b,exp}$
142×60×13×1.3×4.8N90	3.75	3.45	8.10%	4.46	-18.92%
142×60×13×1.3×4.8N120	4.06	3.93	3.23%	4.91	-20.87%

Model number	$R_{b,exp}$ (kN)	Recommended formula R_b (kN)	1-R_b/$R_{b,exp}$	$R_{b,AISI}$	1-$R_{b,AISI}$/$R_{b,exp}$
172×65×13×1.3×5.0N120	4.16	4.15	0.32%	5.43	-30.41%
202×65×13×1.4×5.0N120	5.24	5.19	1.02%	6.51	-24.19%
202×65×13×1.4×5.0N150	5.82	5.69	2.20%	6.91	-18.70%
262×65×13×1.6×5.5N120	5.06	5.52	-9.09%	6.57	-29.88%
262×65×13×1.6×5.5N150	5.37	6.00	-11.68%	6.97	-29.79%
142×60×13×1.3×4.75N30	2.96	2.54	14.11%	3.56	-20.23%
142×60×13×1.3×4.75N60	3.26	2.87	12.11%	3.88	-19.09%
172×65×13×1.3×5.0N32.5	2.88	2.76	4.09%	3.94	-36.78%
172×65×13×1.3×5.0N65	3.31	3.26	1.42%	4.56	-37.65%
202×65×13×1.4×5.0N32.5	3.63	3.27	9.83%	4.30	-18.40%
202×65×13×1.4×5.0N65	4.37	4.28	2.00%	5.61	-28.28%
262×65×13×1.6×5.5N32.5	3.63	3.98	-9.54%	4.87	-34.12%
262×65×13×1.6×5.5N65	3.94	4.38	-11.25%	5.30	-34.47%
302×90×18×2.0×5.5N44	6.95	6.83	1.66%	7.87	-13.29%
Mean of absolute error	—	—	6.35%	—	25.94%

Table 5: Comparison of the results from the recommended formula for the ITF condition and the North American standard formula

Model number	$R_{b,exp}$ (kN)	Recommended formula R_b (kN)	1-R_b/$R_{b,exp}$	$R_{b,AISI}$	1-$R_{b,AISI}$/$R_{b,exp}$
142×60×13×1.3×4.8N30	7.48	7.08	5.39%	10.31	-37.83%
142×60×13×1.3×4.8N60	8.14	7.62	6.41%	11.31	-38.95%
172×65×13×1.3×4.8N32.5	8.92	8.75	1.89%	12.47	-39.83%
172×65×13×1.3×4.8N65	9.48	9.64	-1.73%	13.82	-45.78%
202×65×13×1.4×4.8N32.5	11.46	11.98	-4.51%	15.56	-35.77%
202×65×13×1.4×4.8N65	11.65	12.74	-9.38%	17.06	-46.44%
262×65×13×1.6×5.0N32.5	11.46	13.46	-17.41%	16.14	-40.84%
302×90×18×2×5.0N90	22.31	25.22	-13.05%	29.62	-32.77%
142×60×13×1.3×4.8N90	8.97	8.35	6.90%	12.67	-41.30%
142×60×13×1.3×4.8N120	9.44	9.20	2.56%	13.72	-45.30%
172×65×13×1.3×5.0N120	10.72	10.53	1.74%	16.00	-49.23%
202×65×13×1.4×5.0N150	13.51	14.48	-7.16%	20.58	-52.31%
Mean of absolute error	—	—	6.51%	—	42.20%

5. Conclusion

In this study, the direct strength method (DSM) was applied to the local web bearing problem of cold-formed thin-walled steel components. Based on the virtual work principle, a method for calculating the plastic loads $R_{b,y}$ under the ETF and ITF conditions was derived. The results demonstrated that the formulas were reasonable for the dimensionless ultimate bearing capacity obtained by numerical analysis. The regularised slenderness ratio reasonably reflected the contribution of the web's elastic buckling to the components buckling failure.

Based on the available test data, the results from the proposed formulas were compared with the North American standard calculation values. The values from the proposed formulas were within 10%, while those from the North American standard differed significantly under the ETF and ITF conditions. Therefore, the formulas proposed in this study provide references for engineering applications and specifications revision.

6. Acknowledgments

Supported by National Natural Science Foundation of China 51678476

Supported by Key Research and Development Project of Shaanxi Province 2018ZDXM-SF-097

References

[1] S. Aisi, 100, Specification for the Design of Cold-Formed Steel Structural Members. Washington DC: American Iron and Steel Institute, 2016.

[2] AS/NZS 4600-2018, Cold-Formed Steel Structures. Sydney: Australia: Institute of Steel Construction, 2018.

[3] EN1993-1-3-2006. Eurocode3: Design of Steel Structures, Parts 1-3: General Rules-Supplementary Rules for Cold-Formed Members and Sheeting. European Committee for Standardization, 2006.
[4] B. Young and G. J. Hancock, “Design of cold-formed channels subjected to Web Crippling,” J. Struct. Eng., vol. 127, no. 10, pp. 1137-1144, 2001 [doi:10.1061/(ASCE)0733-9445(2001)127:10(1137)].
[5] B. Young and G. J. Hancock, “Web crippling of cold-formed unlipped channels with flanges restrained,” Thin Walled Struct., vol. 42, no. 6, pp. 911-930, 2004 [doi:10.1016/j.tws.2003.12.001].
[6] M. Macdonald et al., “Web Crippling behaviour of thin-walled lipped channel beams,” Thin Walled Struct., vol. 49, no. 5, pp. 682-690, 2011 [doi:10.1016/j.tws.2010.09.010].
[7] M. A. Heiyantuduwa and M. Macdonald, “A design rule for web crippling of cold-formed steel lipped channel beams based on nonlinear FEA,” Thin Walled Struct., vol. 53, no. 4, pp. 123-130, 2012.
[8] A. P. C. Duarte and N. Silvestre, “A new slenderness-based approach for the web crippling design of plain channel steel beams,” Int. J. Steel Struct., vol. 13, no. 3, pp. 421-434, 2013 [doi:10.1007/s13296-013-3003-4].
[9] P. Keerthan et al., “Web crippling tests of hollow flange channel beams: ETF and ITF load cases”. Australasian Structural Engineering Conf. (ASEC2014), Sky City, Auckland, New Zealand, 2014.
[10] P. Natário et al., “Direct strength prediction of Web Crippling failure of beams under ETF loading,” Thin Walled Struct., vol. 98, no. 1, pp. 360-374, 2016 [doi:10.1016/j.tws.2015.09.012].
[11] P. Natário et al., “Web crippling of beams under ITF loading: A novel DSM-based design approach,” J. Constr. Steel Res., vol. 128, no. 1, pp. 812-824, 2017 [doi:10.1016/j.jcsr.2016.10.011].
[12] P. Natário et al., “Localized web buckling analysis of beams subjected to concentrated loads using GBT,” Thin Walled Struct., vol. 61, no. 12, pp. 27-41, 2012 [doi:10.1016/j.tws.2012.05.014].
[13] P. Natário et al., 2016, “GBTWEB, GBT-based code for web buckling analysis of members under localized loads[CP]”. Available at: http://www.civil.ist.utl.pt/gbtweb.
[14] L. Sundararajah et al., “Experimental studies of lipped channel beams subject to web crippling under two-flange load cases,” J. Struct. Eng., vol. 142, no. 9, p. 04016058, 2016 [doi:10.1061/(ASCE)ST.1943-541X.0001523].
[15] L. Sundararajah et al., “New design rules for lipped channel beams subject to web crippling under two-flange load cases,” Thin Walled Struct., vol. 119, no. 10, pp. 421-437, 2017 [doi:10.1016/j.tws.2017.06.003].
[16] R. R. Gerges and R. M. Schuster, “Web crippling of single web cold-formed steel members subjected to end-one-flange loading,” Proc. 14th International Specialty Conf. on Cold-Formed Steel Structures, St. Louis. S.A.: Missouri U., 1998.
[17] A. Uzzaman, et al, “Cold-formed steel sections with web openings subjected to web crippling under two-flange loading conditions–Part I: Tests and finite element analysis,” Thin Walled Struct., vol. 56, no. 7, pp. 38-48, 2012 [doi:10.1016/j.tws.2012.03.010].
[18] A. Uzzaman, et al, “Web crippling behaviour of cold-formed steel channel sections with offset web holes subjected to interior-two-flange loading,” Thin Walled Struct., vol. 50, no. 1, pp. 76-86, 2012 [doi:10.1016/j.tws.2011.09.009].
[19] B. W. Schafer and T. Pekoz, “Direct strength prediction of cold-formed steel members using numerical elastic buckling solutions” in Proc. Fourteenth International Specialty Conf. on Cold-Formed Steel Structures, 1998, pp. 69-76.
[20] O. Lagerqvist and B. Johansson, “Resistance of I-girders to concentrated loads,” J. Constr. Steel Res., vol. 39, no. 2, pp. 87-119, 1996 [doi:10.1016/S0143-974X(96)00023-5].
[21] N. W. Murray and P. S. Khoo, “Some basic plastic mechanisms in the local buckling of thin-walled steel structures,” Int. J. Mech. Sci., vol. 23, no. 12, pp. 703-713, 1981 [doi:10.1016/0020-7403(81)90008-4].
[22] A. Uzzaman, et al, “Effect of offset web holes on Web Crippling strength of cold-formed steel channel sections under end-two-flange loading condition,” Thin Walled Struct., vol. 65, no. 4, pp. 34-48, 2013 [doi:10.1016/j.tws.2012.12.003].